Loss of Chondroitin Sulfate Modification Causes Inflammation and Neurodegeneration in *skt* Mice

Erica L. Macke,* Erika Henningsen,* Erik Jessen,*,† Nicholas A. Zumwalde,‡ Michael Landowski,* Daniel E. Western,* Wei-Hua Lee,* Che Liu,§, Nathan P. Gruenke,* Anna-Lisa Doebley,* Samuel Miller,* Bikash Pattnaik,††,‡‡,§§ Sakae Ikeda,*,§§ Jenny E. Gumperz,‡ and Akihiro Ikeda*,§§,1**

*Department of Medical Genetics, †Department of Biochemistry, ‡Department of Medical Microbiology and Immunology, §Institute for Molecular Virology, **McArdle Laboratory for Cancer Research, ††Department of Pediatrics, ‡‡Department of Ophthalmology and Visual Sciences, and §§McPherson Eye Research Institute, University of Wisconsin-Madison, Wisconsin 53706

ORCID IDs: 0000-0001-8324-506X (E.L.M.); 0000-0002-5385-358X (B.P.); 0000-0003-1852-2192 (J.E.G.); 0000-0001-8440-3891 (A.I.)

ABSTRACT One major aspect of the aging process is the onset of chronic, low-grade inflammation that is highly associated with age-related diseases. The molecular mechanisms that regulate these processes have not been fully elucidated. We have identified a spontaneous mutant mouse line, small with kinky tail (*skt*), that exhibits accelerated aging and age-related disease phenotypes including increased inflammation in the brain and retina, enhanced age-dependent retinal abnormalities including photoreceptor cell degeneration, neurodegeneration in the hippocampus, and reduced lifespan. By positional cloning, we identified a deletion in chondroitin sulfate synthase 1 (*Chsy1*) that is responsible for these phenotypes in *skt* mice. CHSY1 is a member of the chondroitin N-acetylgalactosaminyltransferase family that plays critical roles in the biosynthesis of chondroitin sulfate, a glycosaminoglycan (GAG) that is attached to the core protein to form the chondroitin sulfate proteoglycan (CSPG). Consistent with this function, the *Chsy1* mutation dramatically decreases chondroitin sulfate GAGs in the retina and hippocampus. In addition, macrophage and neutrophil populations appear significantly altered in the bone marrow and spleen of *skt* mice, suggesting an important role for CHSY1 in the functioning of these immune cell types. Thus, our study reveals a previously unidentified impact of CHSY1 in the retina and hippocampus. Specifically, chondroitin sulfate (CS) modification of proteins by CHSY1 appears critical for proper regulation of immune cells of the myeloid lineage and for maintaining the integrity of neuronal tissues, since a defect in this gene results in increased inflammation and abnormal phenotypes associated with age-related diseases.

KEYWORDS aging; chondroitin sulfate synthase; hippocampus; inflammation; mouse; myeloid cells; neurodegeneration; retina; retinal pigment epithelium; subretinal space

ONE common feature of aging tissues is chronic, low-grade inflammation (Franceschi and Campisi 2014; Fougère *et al.* 2016), which is also observed in multiple age-related diseases such as cardiovascular disease, diabetes, cancer, and neurodegenerative diseases (Danesh *et al.* 2000; Duncan *et al.* 2003; van Greevenbroek *et al.* 2013; Pereira and Alvarez-Leite 2014; Chen and Xu 2015; Zhao *et al.* 2015; Kempuraj *et al.* 2016). There is strong evidence that the low-grade elevation of circulating inflammatory mediators and up-regulation of the inflammatory response play a role in the initiation and progression of these age-related diseases. Mouse models carrying mutations in genes involved in inflammatory signaling show accelerated aging phenotypes (Bernal *et al.* 2014; Franceschi and Campisi 2014; Kõks *et al.* 2016), suggesting the involvement of inflammatory pathways in aging and age-related disease phenotypes. In addition, inhibition of nuclear factor κB (NF-κB)-mediated immune pathways has been shown to result in deceleration of age-related changes (Zhang *et al.* 2013; Yu *et al.* 2014) and increased lifespan in mice (Zhang *et al.* 2013), also pointing to the contribution of inflammation in aging and related detrimental changes to the body. However, the molecular mechanisms that regulate inflammation, aging, and age-related diseases are not fully characterized.

doi: https://doi.org/10.1534/genetics.119.302834
Manuscript received April 15, 2019; accepted for publication November 17, 2019; published Early Online November 21, 2019.
Available freely online through the author-supported open access option.
Supplemental material available at figshare: https://doi.org/10.25386/genetics.10566044.
[1]Corresponding author: Department of Medical Genetics, University of Wisconsin-Madison, Room 5350 Genetics-Biotech, 425-G Henry Mall, Madison, WI 53706. E-mail: aikeda@wisc.edu

Forward genetics approaches using mouse models showing accelerated aging and age-related disease phenotypes provide powerful tools to identify genetic factors involved in aging and age-related diseases (Higuchi *et al.* 2014; Lee *et al.* 2016; Potter *et al.* 2016). These phenotype-driven, unbiased approaches provide an opportunity to identify unexpected factors in various biological pathways that are involved in initiation and progression of the aging process as well as development of age-related pathologies. The retina is an ideal tissue in which to screen for age-related changes, due to its well-organized and layered structure. The normal aging retina goes through a series of distinct pathological changes, including an increase in inflammation, formation of ectopic photoreceptor cell synapses, and degeneration of photoreceptor cells (Liets *et al.* 2006; Aggarwal *et al.* 2007; Eliasieh *et al.* 2007; Terzibasi *et al.* 2009; Samuel *et al.* 2011; Fuchs *et al.* 2012; Zhao *et al.* 2015). Similar retinal abnormalities have been observed in retinal degenerative diseases such as age-related macular degeneration (AMD), suggesting a link between the molecular mechanisms of retinal aging and age-dependent retinal diseases. Elucidating the molecular mechanisms causing these age-dependent retinal abnormalities by utilizing forward genetics may thus enhance our understanding of the molecular and cellular changes underlying aging and age-dependent diseases in the retina, as well as other tissues.

Here, we have identified a mouse model with a spontaneous mutation, small with kinky tail (*skt*), that shows accelerated aging phenotypes in the retina, particularly activation of the retinal innate immune cells, microglia, accompanied by increased retinal stress, synaptic abnormalities, and progressive retinal degeneration. Additionally, we found that *skt* mice exhibit inflammation in multiple other tissues, neurodegeneration in the hippocampus, and reduced life span, suggesting the involvement of the affected molecular pathways in a broader spectrum of age-related symptoms. By positional cloning, we have identified the causative mutation within the gene encoding chondroitin sulfate synthase 1 (*Chsy1*) that plays critical roles in the biosynthesis of chondroitin sulfate (CS), a glycosaminoglycan (GAG), that is attached to the core protein to form the chondroitin sulfate proteoglycan (CSPG) (Mikami and Kitagawa 2013; Kitagawa 2014). Consistent with this finding, we observed a dramatic decrease in CS GAGs within the retina and hippocampus of *skt* mice. In addition, the frequency of macrophages and neutrophils appeared to be markedly reduced in the bone marrow and spleen of *skt* mice. Our results support a novel function for CHSY1 within the retina, brain, and immune cells, and indicate that protein modification by CHSY1 is essential for proper development, function, and/or maintenance of these cells/tissues, such that a defect in this gene results in changes similar to those observed in aging and age-dependent diseases.

Materials and Methods

Mouse husbandry

All experiments were performed in accordance with the National Institutes of Health Guide for the Care and Use of Laboratory Animals and were approved by the Animal Care and Use Committee at the University of Wisconsin-Madison. *skt* mice (STOCK *a skt*/J, stock No: 001433) were obtained from the Jackson Laboratory, crossed to C57BL/6J (B6) mice for one generation and subsequently maintained by intercrossing. We removed the *Ped6b*^{rd1} mutation in the original background known to cause retinal degeneration during this process. C3Sn.BLiA-*Pde6b*$^{+}$/DnJ mice (stock No: 003648) were obtained from the Jackson Laboratory. *Chsy1* knockout (KO) mice (B6;129S5-*Chsy1*^{tm1Lex}/Mmucd) were originally developed by Genentech (Tang *et al.* 2010). Cryo-preserved spermatozoa from heterozygous *Chsy1* KO mice were obtained from the Mutant Mouse Resource & Research Centers (MMRRC; Stock 032195-UCD), and mice were rederived by the Transgenic Animal Facility at the University of Wisconsin-Madison Biotechnology Center.

Histological analysis

Following asphyxiation of mice by CO_2 administration, eyes were immediately removed and immersion fixed in Bouin's fixative overnight at 4°. Eyes were then rinsed, dehydrated, and embedded in paraffin. For histological analysis of the brain, mice were deeply anesthetized with isoflurane and perfused with 4% paraformaldehyde (PFA). Brains were removed and immersion fixed in 4% PFA overnight. Brains were then rinsed, dehydrated, bisected, and embedded in paraffin. Eye sections were cut at 6 μm and brain sections were cut at 15 μm on an RM 2135 microtome (Leica Microsystems, Wetzlar, Germany) and mounted on glass slides. Sections were then stained with hematoxylin and eosin (H&E) to visualize the tissue structure. H&E-stained sections were imaged on an Eclipse E600 microscope (Nikon, Tokyo, Japan), using an Axio Scope.A1 (Carl Zeiss MicroImaging) and an Axiocam 503 color (Carl Zeiss MicroImaging).

Outer nuclear layer thickness measurement

The thickness of retinal layers was measured in H&E-stained sections by using the Measure function of ImageJ software (available at http://rsb.info.nih.gov/ij; developed by Wayne Rasband, National Institutes of Health).

Immunohistochemistry

For cryostat sections, eyes were fixed in 4% PFA for 2 hr at 4°, then cryoprotected at 4° in a graded series of sucrose. Eyes were embedded in optimal cutting temperature compound (Sakura Finetek, Torrance, CA) and sectioned at 12-μm thickness. For immunohistochemistry on cryostat sections, sections were air dried for 2 hr, and blocked in phosphate buffered saline (PBS) with 0.5% Triton X-100 and 2% normal donkey serum for 1 hr at room temperature. Next, sections were incubated overnight with the primary antibodies against the molecule of interest (Supplemental Material, Table S1). Sections were rinsed in PBS and incubated with a 1:200 diluted Alexa 488 conjugated secondary antibody (Thermo Scientific, Rockford, IL) and/or Cy3 conjugated secondary antibody (Jackson ImmunoResearch Laboratories,

West Grove, PA) for 45 min at room temperature. Sections were imaged on a Zeiss 510 confocal laser scanning system using ZEN software (Carl Zeiss MicroImaging) or on a Leica SP8 stimulated emission depletion (STED) 3× microscope (Leica Microsystems, Germany).

Quantification of ectopic dendrites

Frequencies of ectopically localized bipolar cell dendrites extending into the outer nuclear layer (ONL) were quantified in sections immunostained with the protein kinase C (PKC)α antibody, using the Measure and Label function of ImageJ software. We counted the number of PKCα fibers that extended beyond the outer plexiform layer (OPL), and the length was measured along the OPL, using the Measure function of ImageJ software. Frequency was calculated as the number of ectopic bipolar cell dendrites per millimeter of retina length.

Quantification of microglia

Microglia were quantified in sections immunostained with the ionized calcium binding adaptor molecule 1 (Iba1) antibody using the Cell Counter and Measure and Label functions of ImageJ software. We counted the number of total and activated microglia based on morphology as previously described (Jonas *et al.* 2012; Higuchi *et al.* 2014). Activated microglia were defined as cells with a large soma size and no extending processes.

Genetic mapping and next-generation sequencing

Genetic mapping of the *skt* mutation was performed using an F2 intercross (B6;LT-*skt/skt* × C3Sn.BLiA-*Pde6b*$^{+}$/DnJ). A sequence capture array on genomic DNA isolated from the spleen was performed using a biotinylated RNA library created by Agilent, followed by paired end sequencing on the Illumina HiSeq platform DNA Sequencing Facility at University of Wisconsin-Madison Biotechnology Center). Alignment of the sequence reads to the B6 reference genome was performed using the SeqMan NGen software (DNASTAR). The sequence reads covered 93% of bases within the candidate region (an average coverage >100×). Highly repetitive regions were excluded from the capture array and are not represented in this sequence data.

Electroretinogram

Scotopic electroretinogram (ERG) was recorded from 8-week-old *skt* and heterozygous control mice housed in standard diurnal cycling. Mice were dark adapted overnight and ERG recording was performed as previously described (Pattnaik *et al.* 2015). To prevent cataracts, we used tear supplements during handling of mice. Animals were maintained at 37° during the entire procedure. All ERG data were stored and exported in digital format for post-hoc analysis using Microsoft Excel. A two-tailed unpaired Student's *t*-test was used to determine statistical significance. Results are presented as the mean ± SEM and were considered significant for P (P-value) <0.05.

Genotyping

Primers were designed using Primer3. Primer pair F1/R1 was used to amplify the left-hand boundary of the deletion, and F2/R2 to amplify the right-hand boundary. F1 and R2 were used to span the deletion. Primer sequences are as follows:

F1: ctggggcagcagatctattt
F2: tcctggctcctgaatgtctt
R1: gctccaacaccctaggtcag
R2: caactcgatgtagccagcaa

Western blotting analysis

Mouse brains were sonicated in PBS containing a protease and phosphatase inhibitor cocktail (Thermo Scientific, Rockford, IL), then centrifuged at 12,500 rpm for 15 min at 4°. Supernatant was collected and protein was quantified using the Pierce BCA Protein Assay (Thermo Scientific, Rockford, IL) according to the manufacturer's instructions. Primary antibodies to CSPG core proteins (aggrecan, brevican, versican) required samples to be pretreated with 0.2 U/ml chondroitinase ABC (Amsbio) overnight at 37°. The whole brain lysates containing equal amounts of protein were subjected to SDS–PAGE using 10% Bis-Tris gels and primary antibodies (Table S2). IRDye 800CW or IRDye 680RD secondary antibodies were used (LI-COR Biotechnology, Lincoln, NE) prior to detection with the Odyssey CLx imaging system (LI-COR Biotechnology, Lincoln, NE).

Flow cytometry

Bone marrow from femurs and spleen were collected from 8-week-old *Chsy1*^{skt} mutants and heterozygous controls for flow cytometry. Cells were washed with PBS, blocked with 5% mouse serum (abcam, Cambridge, UK) for 15 min, stained with fluorochrome-conjugated antibodies (Table S3) for 30 min at 4°, washed, resuspended in PBS, and analyzed by flow cytometry (BD LSR II cytometer; BD Biosciences, San Jose, CA) with FlowJo analysis software (version 9.3.1; FlowJo, Ashland, OR).

Apoptosis assay

Terminal deoxynucleotidyl transferase dUTP nicked-end labeling (TUNEL) staining was performed with an Apoptag kit using fluorescein detection (Millipore, Billerica, MA), according to the manufacturer's instructions. Nuclei were counterstained with DAPI, and specimens mounted in ProLong Gold antifade reagent (Thermo Fisher Scientific, Waltham, MA). The number of apoptotic cells per retina was counted to obtain a TUNEL positive cells value/retina section/mouse.

Statistical analysis

Sample size was chosen empirically following previous experience in the assessment of experimental variability. No statistical methods were used to predetermine sample size. No animals were excluded. Statistical analyses were performed in GraphPad Prism 6 (RRID:SCR_002798, GraphPad Software,

La Jolla, CA). The statistical difference between groups was calculated using the unpaired Student's two-tailed *t*-test, and ANOVA using the GraphPad Prism software. $P < 0.05$ was considered to be statistically significant, using $^{*}P < 0.05$, $^{**}P < 0.01$, $^{***}P < 0.001$, and $^{****}P < 0.0001$. All data are presented as the mean ± SEM of three or more independent experiments, with three or more replicates per condition per experiment.

Data availability

Strains are available upon request. The authors affirm that all data necessary for confirming the conclusions of the article are present within the article, figures, tables, and supplemental information. Supplemental material available at figshare: https://doi.org/10.25386/genetics.10566044.

Results

Age-related retinal phenotypes in skt mice

The recessive mutation, *skt*, arose spontaneously in a mouse colony at the Jackson Laboratory (Lane 1988). *Skt* mice were originally isolated based on the shorter, kinked tail and small body size (Lane 1988). We found that *skt* mice exhibit abnormalities in the retina, which are similar to age-dependent phenotypes reported in our previous publications (Higuchi *et al.* 2014; Lee *et al.* 2016). Age-dependent retinal phenotypes observed at early ages (by 4–8 weeks) in *skt* mice include ectopic synaptic interaction between photoreceptor cells and bipolar cells detected as mislocalized PKCα-stained biopolar cell dendrites and postsynaptic density protein 95 (PSD95)-labeled photoreceptor presynaptic terminals (Figure 1A, arrowheads), progressive photoreceptor cell degeneration, which was indicated by decreased ONL thickness (Figure 1B and Figure S1A) as well as number of DAPI-stained nuclei in the ONL (Figure S1B), increased apoptosis (Figure 1C), and an increase of glial fibrillary acidic protein (GFAP) expression (Figure 1D), which is considered a sign of retinal stress (Lewis and Fisher 2003) and has been associated with retinal aging in mice (Higuchi *et al.* 2014; Lee *et al.* 2016). These results indicate that age-dependent retinal changes may be accelerated in *skt* mice.

Increased inflammation in the skt retina

Since the retinal innate-immune system involving microglia is known to undergo low levels of activation (para-inflammation) during aging (Chen and Xu 2015), we immunofluorescently stained the retina of 4- and 8-week-old *skt* mice and heterozygous controls for a microglial marker, Iba1, and quantified the total number of microglia. *skt* mice had an overall increase in total microglia beginning at 4 weeks of age and persisting past 8 weeks (Figure 1, E and F). To determine if microglia observed in *skt* mice were activated or resting, we quantified resting, activated, and transitioning microglia based on morphology. Microglia with a small soma and ramified processes were classified as resting, microglia with a large soma and no ramified processes were classified as activated, and microglia with a large soma and few processes extending in a specific direction were classified as transitioning (Jonas *et al.* 2012). *Skt* mice exhibited an increase in both activated and transitioning microglia, indicating an inflammatory status (Figure 1G). These activated microglia were concentrated in the OPL and ONL at 4 weeks of age and shifted to the ONL and retinal pigment epithelium (RPE) at 8 weeks of age (Figure 1E), indicating that the RPE could be the target toward which activated microglia migrate. Similar migration of microglia from the inner retina to the outer retina and their activation have been observed during aging in mice (Xu *et al.* 2008).

Other aging phenotypes in skt mice

Since we observed a broader spectrum of phenotypes associated with aging in *skt* mice including reduced lifespan (Figure S1C), hunched posture, and hair loss with age (Figure S1D) as well as evidence of inflammatory infiltrates in other tissues including the kidney (Figure S1E), we then examined another neuronal tissue, the brain. We performed gross histological examination of various brain regions by H&E staining and found that hippocampal neurons in *skt* mice have undergone significant degeneration by the age of 1.5 years (Figure 2). We observed an increased number of empty spaces surrounding cells in the cornu ammonis 1, 2, and 3 (CA1, CA2, CA3) hippocampal subfields of *skt* mice compared to control mice (Figure 2A). We also observed condensed nuclei in these hippocampal regions of *skt* mice (Figure 2A, arrowheads), indicative of cell death. We immunostained hippocampal neurons using the wolframin ER transmembrane glycoprotein (WFS1) antibody and found that the number of WFS1-positive neurons is significantly reduced in the hippocampus of *skt* mice compared to control mice (Figure 2B, $P = 0.003$ by *t*-test), suggesting degeneration of these neurons. Since microglia, which are increased in the retina (Figure 1), are also associated with neurodegeneration and aging in the hippocampus (Choi *et al.* 2007; Adachi *et al.* 2010; Lee *et al.* 2010), we examined the number of microglial cells in the hippocampus of *skt* mice. We observed an increased number of Iba-positive microglia in the CA1, CA2, and CA3 regions at 1.5 years of age, suggesting increased inflammation in the brain of *skt* mice (Figure 2C and Figure S2A). Quantification of resting, activated, and transitioning microglia based on morphology showed that activated and transitioning microglia are increased in the hippocampus of *skt* mice (Figure S2B). This increase in microglia was observed by 8 weeks of age (Figure S2, A and B and Figure S3A), when morphological changes were not present (Figure S3B). Since inflammation occurs prior to neurodegeneration, increased inflammation could potentially contribute to neurodegeneration in hippocampus.

The Chsy1 gene is mutated in skt mice

To understand the molecular basis of age-dependent abnormalities observed in *skt* mice, we conducted positional cloning. Genetic mapping of the *skt* mutation was performed

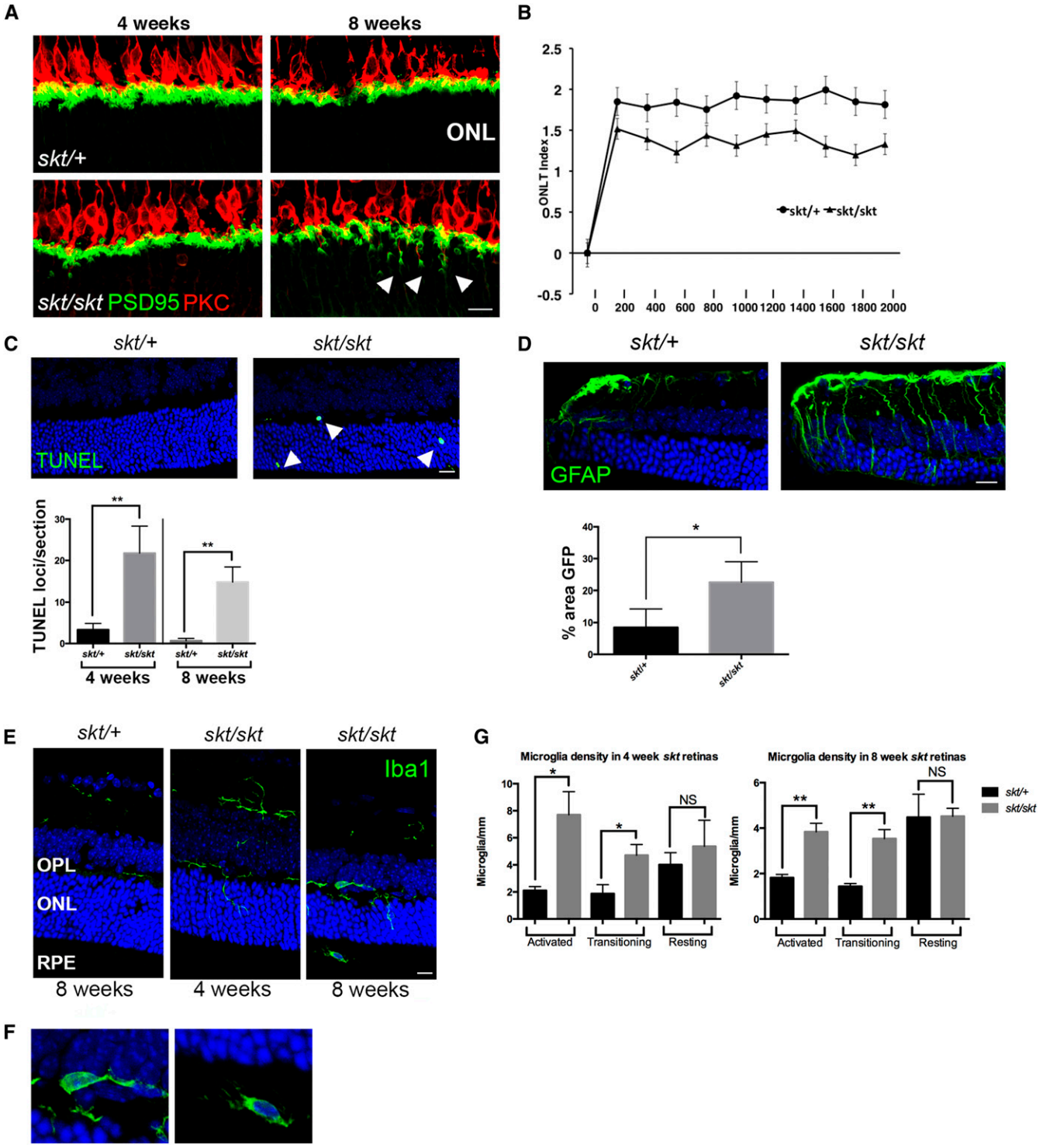

Figure 1 (A) PKCα-labeled (red) bipolar cell dendrites and PSD95-labeled (green) photoreceptor presynaptic terminals are mislocalized in the outer nuclear layer (ONL) of *skt* mice at 8 weeks of age. Bar, 10 μm. (B) Decreased ONL thickness in 8-week-old *skt* mutant retina indicating photoreceptor cell degeneration ($n = 5$ per genotype). (C) Increased photoreceptor cell death in the *skt* retina. Retinal sections from 4-week-old *skt* and heterozygous control mice show TUNEL staining (green) in the ONL of *skt* mice (arrowheads). Sections are counterstained with DAPI (blue). Bar, 10 μm. *skt* mice exhibit a significant increase in TUNEL positive loci (expressed as number of TUNEL positive loci per retinal section in the graph) at 4 and 8 weeks of age ($n = 5$ per genotype). $^{**}P < 0.01$. (D) Increased stress in the *skt* retina indicated by GFAP (green) staining. Sections are counterstained with DAPI (blue). Bar, 10 μm. At 8 weeks of age *skt* mutants exhibit a significant increase in GFAP staining (expressed as % area covered by GFAP staining in the graph), indicating increased retinal stress ($n = 5$ per genotype). $^{*}P < 0.05$. (E) Microglia invasion in the retina. Iba1 staining (green) on 4- and 8-week-old retinal samples shows invasion of microglial cells into the outer plexiform layer (OPL), ONL, and retinal pigment epithelium (RPE) of *skt* mice. Sections are counterstained with DAPI (blue). Bar, 10 μm. (F) Higher magnification views of microglia in the *skt* retina at 8 weeks of age. (G) *skt* mice exhibit a significant increase of activated and transitioning microglia at 4 weeks (left) and 8 weeks (right) of age ($n = 5$ per genotype). $^{*}P < 0.05$; $^{**}P < 0.01$.

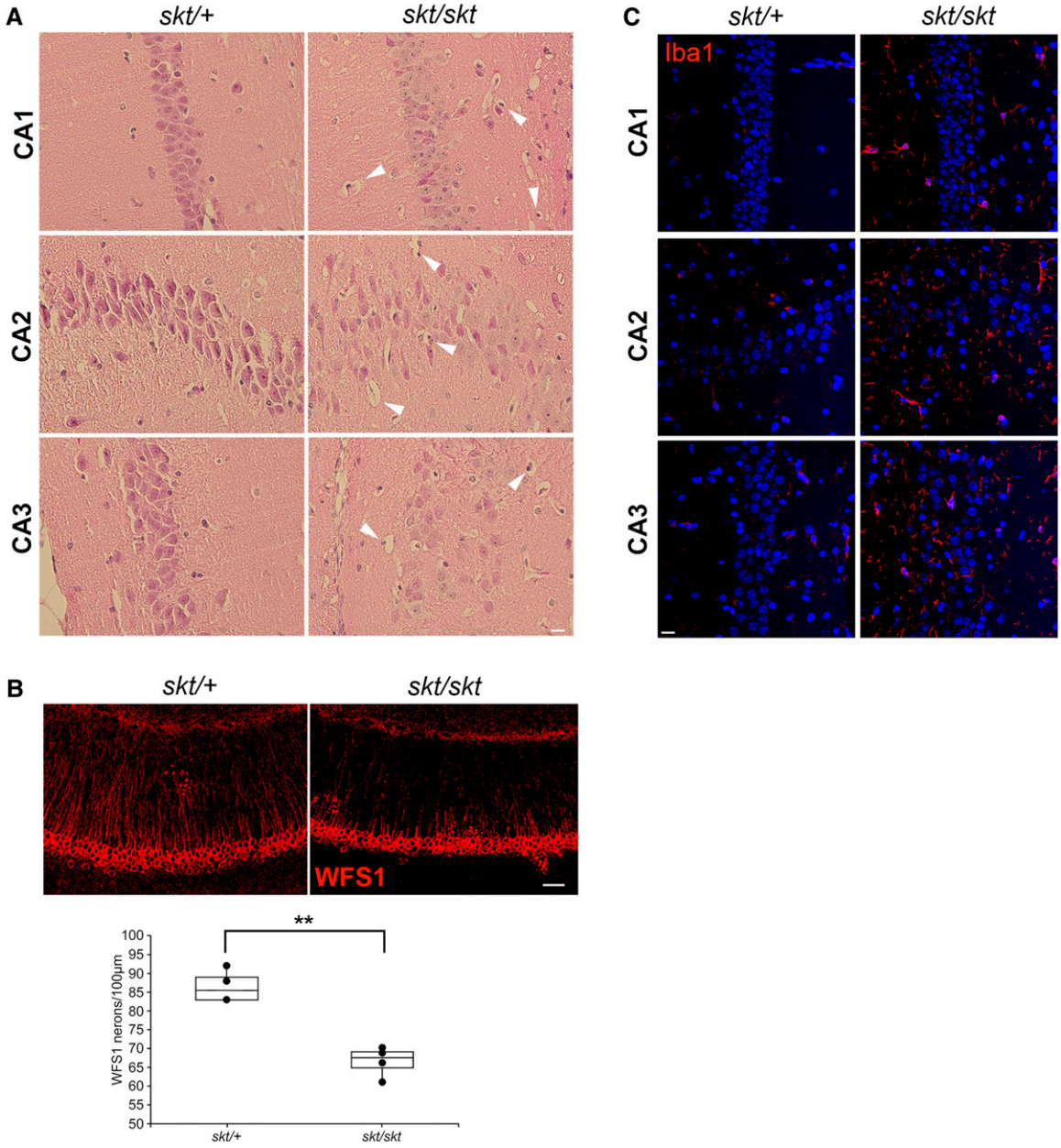

Figure 2 (A) Neurodegeneration in the *skt* hippocampus. H&E staining of brain sections from 1.5-year-old *skt* and heterozygous control mice indicated neurodegeneration in the CA1, CA2, and CA3 hippocampal regions of *skt* mice. Shrinkage of cells, empty spaces, and condensed nuclei (arrowheads) are observed within all regions indicating cell death. (B) *Skt* mice exhibit a decrease in the number of WFS1 (red)-positive neurons in the hippocampus at 1.5 years of age ($n = 4$ per genotype). $^{**}P < 0.01$. Bar, 10 μm. (C) Microglia (Iba1, red) are increased in the *skt* brain at 1.5 years of age, visible in the CA1, CA2, and CA3 regions of the hippocampus. Sections are counterstained with DAPI (blue). Bar, 10 μm.

using an F2 intercross (B6/LT-*skt/skt* × C3Sn.BLiA-*Pde6b*$^{+}$/DnJ). *skt* was mapped to a 2.5-Mb region on mouse chromosome 7 flanked by markers D7Mit89 and D7Mit231 (Figure 3A). We then performed a sequence capture array on genomic DNA from *skt* mutants ($n = 2$). Standard bioinformatic analysis revealed no single-nucleotide polymorphisms (SNPs) nor small insertions and deletions within the coding regions (Table S4). Coverage analysis identified an area of zero coverage located at the three prime end of *Chsy1* (Figure 3B), indicating a possible insertion or deletion. Discarded reads from the original alignment were analyzed to identify reads bordering the no coverage region (Figure 3, C and D). All 48 discarded reads contained sequence data that align to *Chsy1*, and a DNA sequence matching a region 27,666 bp downstream of *Chsy1*, indicating a large deletion (Figure 3D). PCR products were amplified from wild-type and heterozygote genomic DNA using primers spanning the left (F1/R1) and right (F2/R2) boundaries of the deletion (Figure 3E), which failed to amplify from genomic DNA of *skt* mutants (Figure 3F). Additionally, we are able to amplify a 200-bp

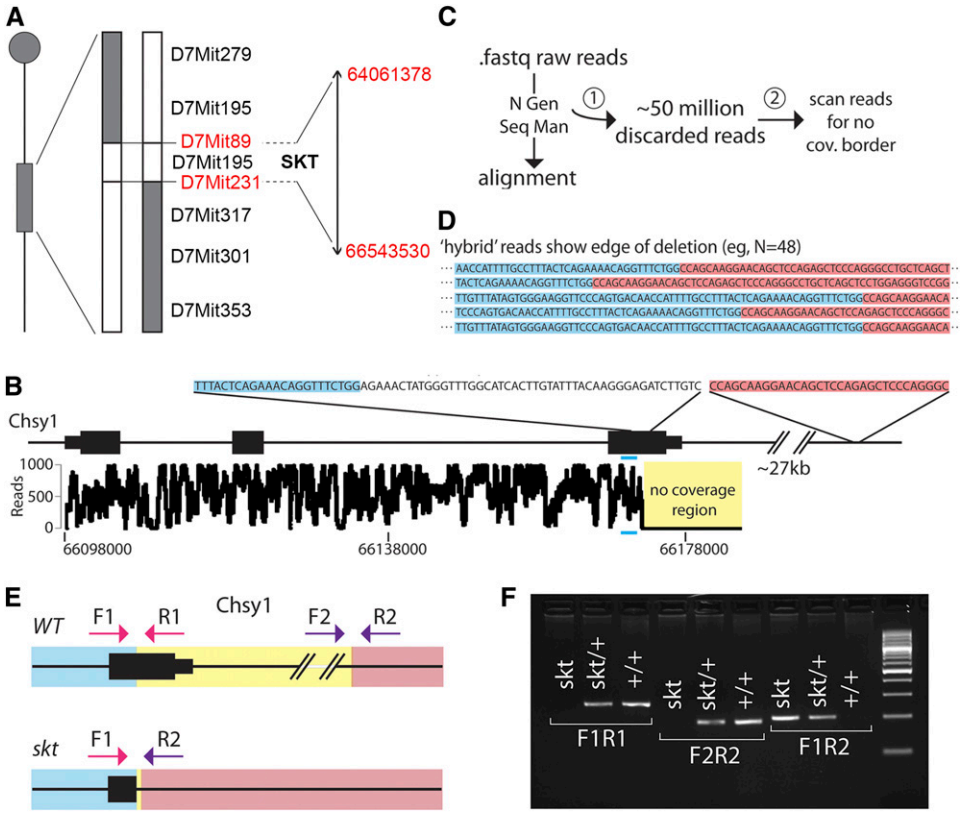

Figure 3 Identification of the *skt* genomic deletion. (A) The *skt* locus has been mapped to a 2.5-Mb region located on mouse chromosome 7 flanked by D7Mit89 and D7Mit231. (B) Sequence coverage of the *Chsy1* gene. No coverage region is shown at the 3′ end of the *Chsy1* gene (yellow). (C) Data pipeline used to identify the genomic deletion. The raw sequence reads were aligned to the mouse mm10 reference genome using the SeqMan N Gen suite software. The discarded reads were saved in a .fas file (1). An in-house perl script was used to scan and pull discarded reads that contained the sequence of the *Chsy1* region adjacent to the start of the no coverage region (blue) at the 3′ end of *Chsy1* (2). (D) Forty-eight discarded reads were identified to overlap the deletion, containing the sequence adjacent to the no coverage region, and a DNA sequence that was identified to be 27,666bp downstream of *Chsy1* (red). The wild-type sequence is shown down below the reads. (E) Design of primer sets F1/R1 and F2/R2 to confirm the skt deletion. F1/R1 spans the left-hand boundary of the deletion, while primer set F2/R2 spans the right-hand boundary. (F) A 250-bp product (F1/R1) and a 190-bp product (F2/R2) can be amplified from heterozygote and wild-type samples. Due to the deletion, these primer pairs do not amplify products from *skt* DNA. Using the primer pair F1/R2, a 200-bp product can be amplified from heterozygote and homozygous *skt* DNA.

product from heterozygotes and *skt* mutant DNA using primers F1 and R2 spanning the 27-kb deletion, which is not amplified from wild-type DNA (Figure 3F). These results indicate that a 27-kb deletion exists within the *Chsy1* gene in *skt* mice. Since this deletion affects the functionally important chondroitin N-acetylgalactosaminyltransferase (CHGN) domain of CHSY1 (amino acid 238–777 in humans) (Li *et al.* 2010), it likely results in loss of function. To confirm *Chsy1* as the causative gene, a complementation test was performed using B6;129S5-*Chsy1*^{tm1Lex}/*Mmucd* (*Chsy1* KO) mice (Wilson *et al.* 2012). Mice heterozygous for the *Chsy1* KO allele and the *skt* allele exhibit an increase in ectopically localized photoreceptor synapses (Figure S4, A and B), decreased ONL thickness (Figure S4C), an increase in microglia (Figure S4D), decreased body size, and a kinked tail (Figure S4E). These data show that the *skt* mutation is indeed in the *Chsy1* gene, and further indicate that it is a loss-of-function mutation. Hereafter, we designate the *skt* mutation as *Chsy1*^{skt}.

Decreased CS GAGs in the outer retina and brain of Chsy1^{skt} *mice*

CHSY1 is a member of the chondroitin N-acetylgalactosaminyltransferase family (Kitagawa *et al.* 2001) that synthesizes CS, a GAG expressed on the surface of most cells and in the extracellular matrix (Mikami and Kitagawa 2013). It catalyzes the addition of alternating GalNAc and GlcA disaccharide units to elongate CS chains attached to the core protein-forming CSPGs (Figure 4A). In the retina, CSPGs were previously detected in large quantities in the interphotoreceptor matrix (IPM), which occupies the subretinal space between the photoreceptor cells and RPE cells, as well as on the apical surface of RPE cells (Porrello and Lavail 1986; Hageman and Johnson 1987; Ishikawa *et al.* 2015). We performed immunohistochemistry with antibodies targeting CHSY1 and 4-sulfated or 6-sulfated CS GAGs of CSPGs in the retina of *Chsy1*^{skt} and control mice. In the outer retina of both *Chsy1*^{skt} and control mice, CHSY1 was detected in the RPE as well as photoreceptor inner segments (IS) (Figure 4B). CS GAGs are localized primarily to the photoreceptor outer segments (OS) and the apical region of RPE in control mice, which is absent in *Chsy1*^{skt} mutants (Figure 4B). This indicates a significant impairment of CS modification in these retinal regions of *Chsy1*^{skt} mice, which may affect their structural integrity. Immunofluorescence for rhodopsin shows disrupted OS morphology in *Chsy1*^{skt} mice (Figure 4C). While columnar structures of the OS are well defined and OS tips can be clearly observed in the control retina using STED microscopy, they are severely disorganized and undefined in *Chsy1*^{skt} mice (Figure 4C). Additionally, signals for solute carrier family 16 (monocarboxylic acid transporters) member 1 (SLC16A1), an apical marker of RPE cells, are much less intense in *Chsy1*^{skt} mutants (Figure 4D) suggesting that RPE microvilli may be affected in these mice. These structural defects at the interface of photoreceptor and RPE cells may indicate abnormal interaction between these cells. We hypothesized that these structural defects and photoreceptor cell degeneration observed in

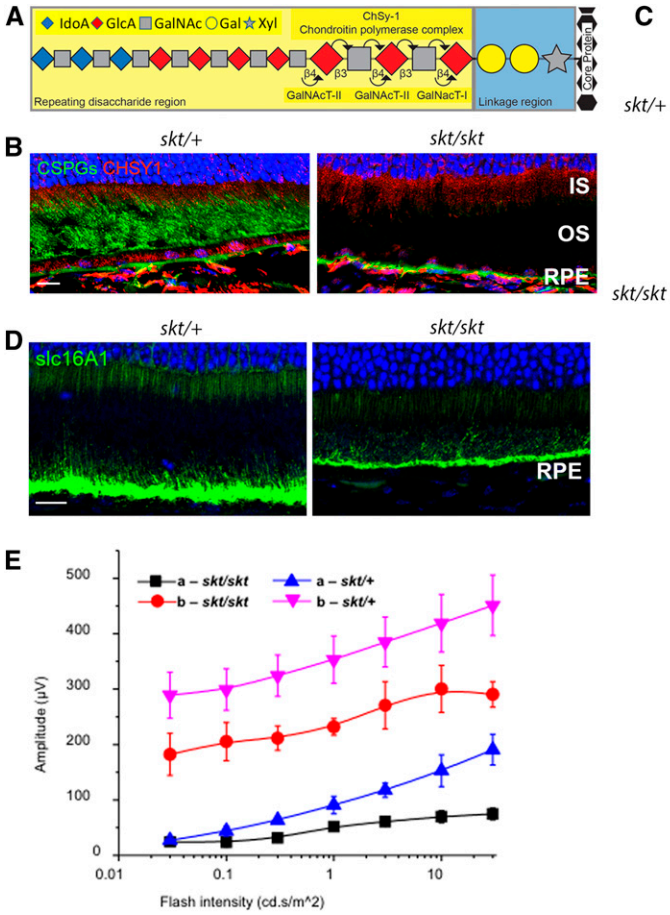

Figure 4 (A) Chondroitin sulfate is a sulfated glycosaminoglycan (GAG) composed of a chain of alternating sugars. It is attached to proteins by CHSY1 as part of a proteoglycan. (B) Both *Chsy1*^{skt} and heterozygous control mice exhibit CHSY1 (red) staining in the photoreceptor inner segments (IS) and RPE at 8 weeks of age. CS GAGs (green) are localized primarily to outer segments (OS) and the apical surface of the RPE in controls, but are absent from these regions in *Chsy1*^{skt} mice. Sections are counterstained with DAPI (blue). Bar, 10 μm. (C) OS morphology is severely disrupted in *Chsy1*^{skt} mice compared to control mice in which columnar structures are observed (rhodopsin, white) by STED microscopy. Bar, 5 μm. (D) Signals for the apical RPE marker SLC16A1 (green) are less intense in *Chsy1*^{skt} mutants (n = 5 per genotype). Bar, 10 μm. (E) Functional vision loss in *Chsy1*^{skt} mice is indicated by reduced a and b wave in scotopic ERG at 8 weeks of age ($P < 0.05$ by Student's t-test; n = 4 per genotype).

the *Chsy1*^{skt} mutant could affect the visual function. To test this, scotopic ERG recording was performed on 8-week-old *Chsy1*^{skt} mutants and controls. *Chsy1*^{skt} mice exhibit a significant decrease in both a and b waves (Figure 4E), indicating a functional loss of vision.

In the adult brain, CSPGs are major components of the extracellular matrix (ECM) and have been detected in various regions (Kurazono *et al.* 2001; Galtrey and Fawcett 2007; Hayashi *et al.* 2007). Staining for CHSY1 and for 4-sulfated/6-sulfated CS GAGs of CSPGs generally coincided in the hippocampus (Figure 5, A–C). Similarly to the retina, *Chsy1*^{skt} mice show decreased staining for CS GAGs in the hippocampus compared to control mice (Figure 5D, red), suggesting that the integrity of the ECM surrounding neurons may be affected in *Chsy1*^{skt} mice. We also performed Western blotting analysis on brain lysates from control and *Chsy1*^{skt} mice using the antibody for CS GAGs. We observed a major reduction in CS GAG signals across a range of molecular weights in *Chsy1*^{skt} mice compared to control mice (Figure 5E), suggesting that various CSPGs are generally affected in this mouse model. To examine whether CSPG core protein expression is affected, we performed Western blotting for some of the major CSPG core proteins in the central nervous system including aggrecan, brevican, and versican (Stephenson *et al.* 2018) on brain lysates that were pretreated with the chondroitinase ABC enzyme. We did not find significant differences in signals for these core proteins (Figure 5E), suggesting that while these core proteins are present, their CS modification is disrupted by the *Chsy1*^{skt} mutation. For one of the transmembrane CSPG core proteins, neuron-glial antigen 2 (NG2) (also known as CSPG4), we performed immunohistochemistry in the hippocampus. NG2 is known to be expressed in NG2-glia, precursors of mature oligodendrocytes that reside in the adult brain parenchyma (Jäkel and Dimou 2017). In the hippocampus, NG2 signals (Figure 5D, green) were found to overlap with CS GAG signals (Figure 5D, red), which were reduced in *Chsy1*^{skt} mice. Similarly, NG2 signals were markedly reduced in the retina of *Chsy1*^{skt} mice (Figure 5F). In the control retina, strong NG2 signals were observed at the apical surface of the RPE, which are significantly lower in *Chsy1*^{skt} mice (Figure 5F, green). Since the polyclonal NG2 antibody used for immunohistochemistry detects both the intact proteoglycan and the core protein, reduced NG2 signals in *Chsy1*^{skt} mice could indicate either the loss of antigenic sites due to reduced CS modification (that are present and detected by this antibody in control mice) or instability of the NG2 core protein without CS modification in *Chsy1*^{skt} mice. Therefore, we performed Western blotting of the brain lysate from *Chsy1*^{skt} and control mice using an antibody that was generated against synthetic peptide corresponding to the mouse NG2 amino acid sequence (aa 300–400),

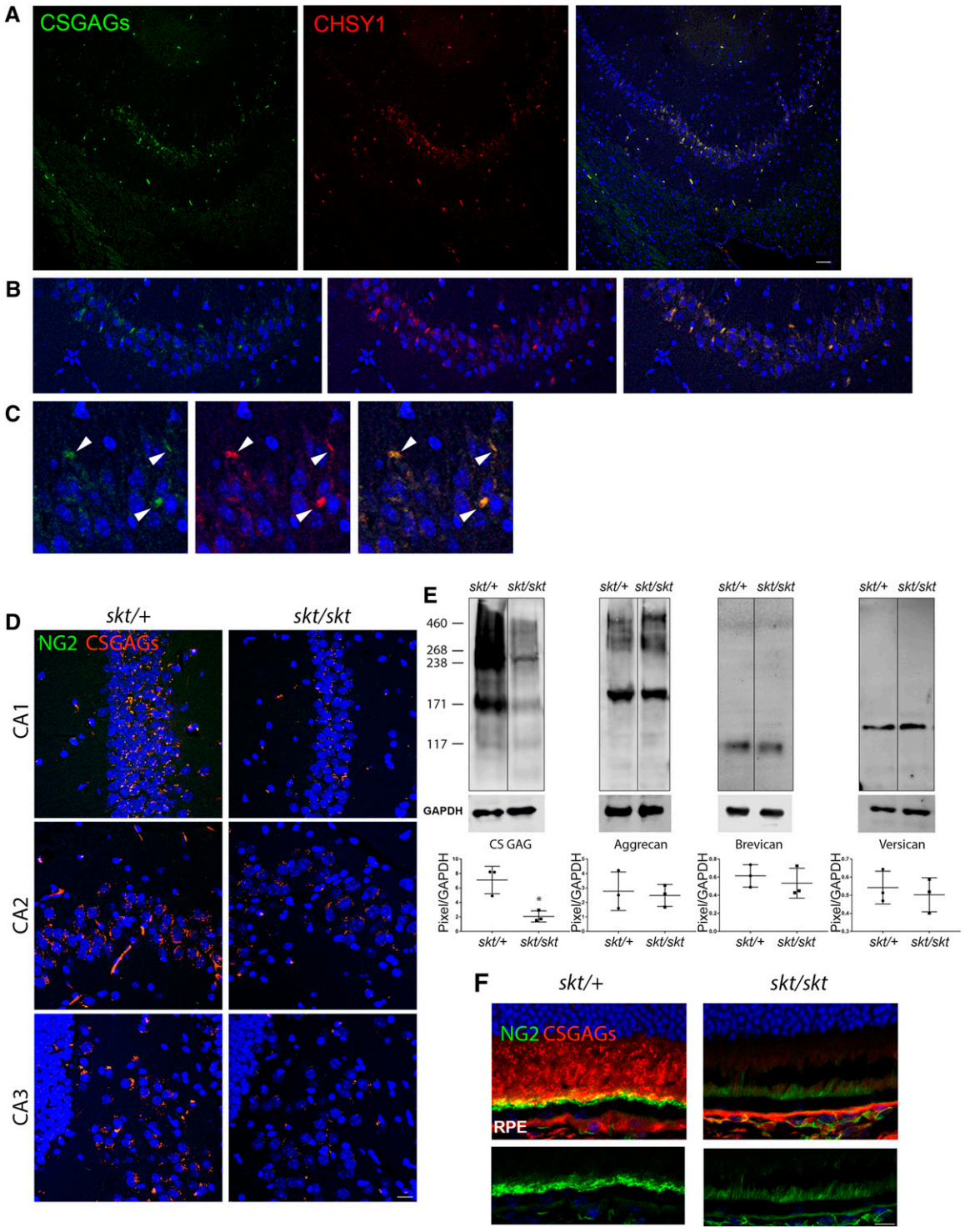

Figure 5 (A) CS GAGs (green) and CHSY1 (red) signals coincide in the hippocampus. Bar, 20 μm. (B and C) Higher magnification views of CS GAGs (green) and CHSY1 (red) signals that are overlapping (arrowheads) in the hippocampus. Sections are counterstained with DAPI (blue). (D) CS GAGs (red) and NG2 signals overlap in the hippocampus, which are reduced in the *Chsy1*$^{skt/skt}$ brain compared to heterozygous (*Chsy1*$^{skt/+}$) controls. Bar, 10 μm. (E) Western blotting analysis of brain lysates from *Chsy1*$^{skt/skt}$ and heterozygous control mice using antibodies against 4-sulfated/6-sulfated CS GAGs and CSPG core proteins (aggrecan, brevican, versican). For the analysis of core proteins, lysates were pretreated with the chondroitinase ABC enzyme. n = 3 for each genotype. Protein levels are shown as normalized to the loading control, GAPDH. $^*P < 0.05$. (F) In the outer retina, NG2 (green) is localized specifically to the apical surface of RPE cells, which is significantly reduced in *Chsy1*$^{skt/skt}$ mice compared to *Chsy1*$^{skt/+}$ control mice. The section is costained with the CS GAGs antibody (red). Bar, 10 μm. Sections are counterstained with DAPI (blue).

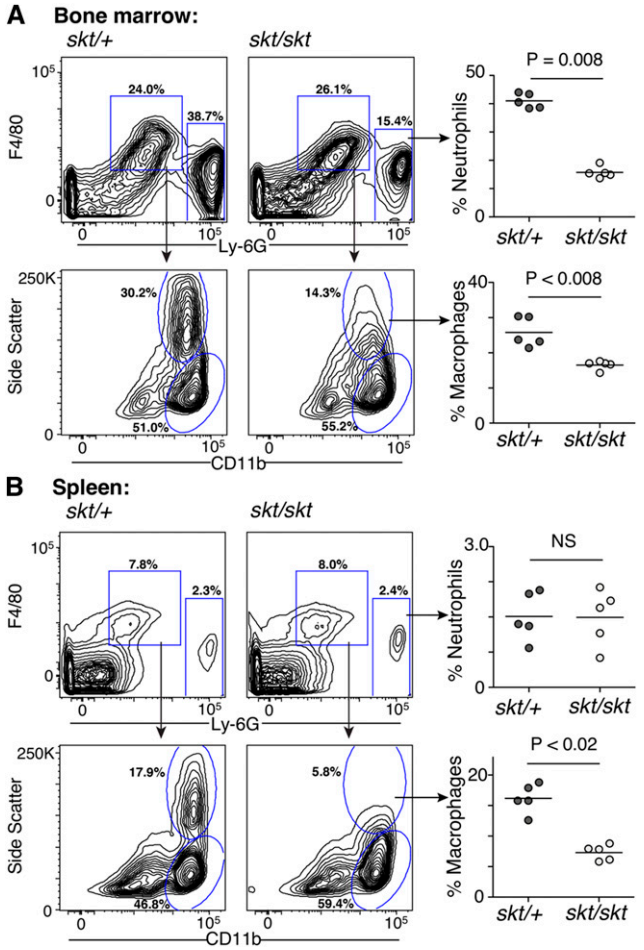

Figure 6 Disruption of immune cell populations in *Chsy1*^{skt} mutants. Flow cytometric analysis of bone marrow (A) and spleen (B) samples from *Chsy1*^{skt} mice compared to heterozygous controls. Top contour plots show identification of neutrophils (Ly-6G^{hi} population) and F4/80^{+} cells. Bottom contour plots show identification of macrophage (CD11b^{+}SSC^{hi}) and monocyte (CD11b^{+}SSC^{med}) subsets within the F4/80^{+} population. Scatter plots on right show aggregated frequencies of neutrophils (top plots) *vs.* macrophages (bottom plots) from five heterozygous (*skt*/+) mice *vs.* five homozygous (*skt/skt*) mice, and demonstrate significantly reduced frequencies of neutrophils and macrophages in bone marrow (A), and of macrophages in spleen (B).

which should recognize the NG2 core protein (Figure S5). This analysis did not show significant difference in the level of the NG2 core protein between *Chsy1*^{skt} and control mice (P = 0.1354 by t-test), indicating that CS modification of the NG2 core protein (and not the level of the NG2 core protein) is specifically affected in *Chsy1*^{skt} mice.

Altered neutrophil and macrophage frequencies in Chsy1^{skt} *mice*

Using a gene annotation portal (bioGPS) (Wu *et al.* 2016), we analyzed the expression pattern of the *Chsy1* gene in mouse tissues and cell types (Lattin *et al.* 2008) and found that it is expressed in immune cell populations. Based on this, we hypothesized that CHSY1 may be involved in the function/regulation of immune cells. We thus performed flow cytometric analyses of immune populations from bone marrow and spleen of 8-week-old *Chsy1*^{skt} mutants and heterozygous controls (Figure 6 and Figures S6 and S7). We first noted a significantly reduced frequency of cells showing high side-scatter (SSC^{high}) in both bone marrow and spleen from *Chsy1*^{skt} mutants (Figure S6). Since myeloid lineage cells such as macrophages and granulocytes are characterized by high side-scatter, we performed further analyses using antibodies against Ly-6G (highly expressed on neutrophils) *vs.* F4/80 and CD11b (both more highly expressed on monocytes and macrophages than neutrophils). The frequency of neutrophils (F4/80^{low}, Ly-6G^{high}) appeared significantly reduced in bone marrow of *Chsy1*^{skt} mutants compared to heterozygous controls, but was not affected in spleen (Figure 6). The macrophage subset (F4/80^{+}, CD11b^{hi}, SSC^{hi}) appeared markedly diminished in both bone marrow and spleen of *Chsy1*^{skt} mutants compared to heterozygous controls (Figure 6). In contrast, frequencies of monocytic cells and lymphocytic cell types [including T-cells, B-cells, and natural killer (NK) cells] did not appear to be consistently altered in *Chsy1*^{skt} mutants compared to heterozygous controls (Figure S7). These results suggest that CHSY1 may have a role in the generation, maintenance, or tissue localization of neutrophils and macrophages.

Discussion

In this study, we identified *Chsy1* as the responsible gene for *skt* mutant phenotypes including accelerated age-dependent retinal abnormalities, neurodegeneration in hippocampus, and inflammation in multiple tissues. Specifically, we found a large deletion beginning in the third exon of *Chsy1*, spanning 27 kb into the intergenic space. CHSY1 is a member of the chondroitin N-acetylgalactosaminyltransferase family (Kitagawa *et al.* 2001). These enzymes possess dual glucuronyltransferase and galactosaminyltransferase activity and play critical roles in the biosynthesis of CS, a GAG, that is attached to a serine residue of the core protein to form CSPGs (Mikami and Kitagawa 2013; Kitagawa 2014). In humans, mutations in *CHSY1* have been associated with Temtamy preaxial brachydactyly syndrome, characterized by limb malformations, short stature, and hearing loss (Li *et al.* 2010; Tian *et al.* 2010; Sher and Naeem 2014). A previous study using *Chsy1* KO mice showed that CHSY1 is required for bone development and digit patterning (Wilson *et al.* 2012). *Chsy1* KO mice also exhibit a kinked tail, similarly to *Chsy1*^{skt} mutants, likely due to abnormalities during bone development. We confirmed that *Chsy1*^{skt} is allelic to the *Chsy1* KO allele by complementation test, which also indicated that *Chsy1*^{skt} is a loss-of-function mutation. Thus, our study revealed previously unidentified tissues/cell types that are affected by the loss of CHSY1 function including the retina, hippocampus, and immune cells. Moreover, we discovered that defects in CS modification by CHSY1 result in increased inflammation and abnormal phenotypes associated with aging and age-related diseases.

Our immunohistochemical analysis showed that CS GAGs in the IPM of the retina are dramatically decreased in *Chsy1*^{skt} mice. The significant reduction of CS modification in this region prompted us to further examine the photoreceptor OS structure, which appeared less defined and disorganized. We also found that RPE microvilli that surround the OS tips are affected in *Chsy1*^{skt} mice. Thus, our data demonstrate that CHSY1 is an essential enzyme for production of CSPGs in IPM, and that CSPGs in this retinal region are essential for structural integrity of OS and RPE microvilli at the interface between photoreceptor–RPE interaction. Defective interaction could affect the health/maintenance of photoreceptor cells and visual functions, consistent with our data showing progressive photoreceptor cell degeneration and impaired ERG responses in *Chsy1*^{skt} mice. Additionally, our data demonstrate that activated microglia migrate toward the OS/IPM and RPE as the *Chsy1*^{skt} phenotype progresses, indicating that these structural defects due to loss of CS modification may induce activation and recruitment of microglia. Microglia-mediated chronic neuroinflammation has been observed in multiple retinal degenerative diseases including AMD, glaucoma, and diabetic retinopathy, as well as mouse models with retinal degeneration, and is thought to have a pivotal role in the degenerative process (Langmann 2007; Karlstetter *et al.* 2010; Madeira *et al.* 2015). Considering that increase in activated microglia is one of the earliest phenotypes observed in the *Chsy1*^{skt} retina, it is possible that this phenomenon contributes to retinal degeneration in *Chsy1*^{skt} mice.

Our histological data indicate significant neurodegeneration within the *Chsy1*^{skt} hippocampus. Within the brain, CSPGs are the most abundant part of the ECM and different types of CSPGs are localized to intercellular spaces between neurons and glia (Dityatev *et al.* 2007; Bonneh-Barkay and Wiley 2009; Maroto *et al.* 2013). Additionally, perineuronal nets (PNNs) are CSPG-rich ECM lattice-like structures that envelop subpopulations of neurons in certain brain regions including the hippocampus (Celio and Blümcke 1994; Deepa *et al.* 2006; Maroto *et al.* 2013) and play key roles in neural development, synaptogenesis, neuroprotection, and synaptic plasticity. The degeneration we observed in the *Chsy1*^{skt} hippocampus indicates that modification of proteins by CHSY1 is important for maintaining neuronal health in the brain, and lack of those CS modifications can lead to neurodegeneration. Results from our Western blotting analysis indeed indicated general reduction in CS modification of CSPGs while levels of core proteins for major CSPGs were not affected in the brain of *Chsy1*^{skt} mice, indicating that CS modification of the core proteins is specifically reduced in these mice. Similarly to the retina, it is plausible that structural changes within the ECM due to loss of CS modification of CSPGs lead to neurodegeneration within the brain. The ECM in the brain is thought not only to provide physical support but also to support homeostatic functions required for survival of neurons (Bonneh-Barkay and Wiley 2009). Changes in the ECM have been associated with neurodegenerative diseases including ischemic stroke, multiple sclerosis, human immunodeficiency virus dementia and AD, and animal models of such diseases (Bonneh-Barkay and Wiley 2009), although a mechanistic connection has not been fully demonstrated. Alternatively, neuroinflammation involving microglia may contribute to neurodegeneration. Our study shows that the number of activated microglial cells is increased in the *Chsy1*^{skt} brain. Since activation of microglia has been associated with neurodegeneration (Perry and Holmes 2014; Brown and Vilalta 2015; von Bernhardi *et al.* 2015; Colonna and Butovsky 2017), increased microglia and their activation may contribute to hippocampal degeneration observed in *Chsy1*^{skt} mice. The ECM is known to modulate immune cell migration, activation, and survival (Sorokin 2010), and inflammation can be initiated and propagated by ECM disruption (Gaudet and Popovich 2014). Therefore, disruption of the ECM due to the loss of CS modification may increase neuroinflammation in the *Chsy1*^{skt} brain, which may in turn result in neurodegeneration.

Our Western blot analysis showed general reduction in CSPG signals across a range of molecular weights in *Chsy1*^{skt} brain, suggesting that the *Chsy1*^{skt} mutation affects various CSPGs. In previous studies, no apparent degeneration or inflammation in the brain was reported in mice lacking major CSPGs in the central nervous system (CNS), neurocan (Zhou *et al.* 2001) or brevican (Brakebusch *et al.* 2002), as well as in quadruple knockout mice lacking neurocan, brevican, and glycoproteins tenascin-C and tenascin-R (Rauch *et al.* 2005). Closer examination of the hippocampus of these mouse models may reveal inflammation and/or degenerative phenotypes, which would indicate their involvement. We also found a candidate transmembrane CSPG, NG2, that may be involved, since it was detected in regions of both retina and brain where *Chsy1*^{skt} phenotypes were observed. In the outer retina, NG2 signals were observed specifically at the apical surface of the RPE cells in control mice, while in the hippocampus of control mice, they were found to overlap with CS GAG signals. In *Chsy1*^{skt} mice, NG2 signals in both tissues were much reduced compared to those in control mice. Future studies to identify CSPGs that are responsible for particular *Chsy1*^{skt} phenotypes should provide valuable insights regarding the molecular mechanisms underlying the pathologies.

We found that macrophage and neutrophil populations in bone marrow, and macrophages in the spleen, appeared significantly diminished in *Chsy1*^{skt} mice. Thus, our study shows that CS modification of proteoglycans affects the development, maintenance, or localization of myeloid subsets, particularly macrophages. Microglia are known to be CNS-resident macrophages that arise early in development from the yolk sac; however, the extent to which bone marrow-derived macrophages also infiltrate the CNS later in life as part of the normal course of aging remains unclear (Lund *et al.* 2017; Mrdjen *et al.* 2018). It is therefore intriguing to speculate on whether the neuroinflammatory phenotype observed in *Chsy1*^{skt} mice is connected to their deficiency in bone marrow macrophages, since this might suggest an unexpected role for bone marrow-derived macrophages in protecting against age-related inflammatory pathology in

the CNS. Notably, a human GWAS study has shown association of SNPs within *CHSY1* to the count/percentage of myeloid lineage cells (Astle *et al.* 2016), consistent with our findings in *Chsy1*^{skt} mice. Expression of CHSY1 has been detected in multiple immune cell types (Lattin *et al.* 2008) including NK cells, mast cells, B-cells, T-cells, dendritic cells, macrophages, and microglia. Hence, loss of this gene may affect a variety of immune cell types, and *Chsy1*^{skt} mice may provide a novel mouse model to study how CS modification of proteoglycans is involved in the regulation of immune cell populations.

In conclusion, our study revealed the importance of CS modification with wider roles in regulating immune cells/inflammation affecting multiple organ systems. Loss of CS modification also results in neurodegeneration in the retina and hippocampus demonstrating the importance of CS modification by CHSY1 for the maintenance of those neurons. Two separate hypotheses exist regarding neurodegeneration in *Chsy1*^{skt} mice. It may result from structural changes in the ECM surrounding the neurons due to reduced CS modification of CSPG core proteins. Alternatively, it may be due to immune cells affected by the *Chsy1*^{skt} mutation resulting in inflammation and neurodegeneration. Future investigation will test these hypotheses. Furthermore, although it is not known whether age-dependent changes in CS are involved in increased inflammation or neuronal degeneration associated with aging, changes in CS modification in some aging tissues have been reported (Collin *et al.* 2017; Foscarin *et al.* 2017). A significant decrease in CS GAGs as well as changes in the sulfation profile of CS were observed in the bovine intervertebral disc during the aging process (Collin *et al.* 2017). Changes in the sulfation pattern of CS were also observed in aged rat brains, which may have a more inhibitory effect on axon growth (Foscarin *et al.* 2017). Such age-dependent changes in CS modification may more generally occur in different tissues. Importantly, our study demonstrated that global changes in CS modification could contribute to the development of aging and age-related disease phenotypes. Future identification of the targets of CS modification by CHSY1 and cell types that are specifically responsible for causing the age-related disease phenotypes could provide further insights into the molecular mechanisms through which these pathologies associated with aging and age-related diseases are caused.

Acknowledgments

We thank Satoshi Kinoshita for generation of frozen sections and Lance Rodenkirch for assistance with confocal imaging. The mouse strain used for this research project, B6;129S5-*Chsy1*$^{tm1Lex/Mmucd}$, identification number 032195-UCD, was obtained from the Mutant Mouse Regional Resource Center (MMRRC), a National Center for Research Resources (NCRR)-National Institutes of Health (NIH)-funded strain repository, and was donated to the MMRRC by Lexicon Genetics Incorporated. This work was supported by National Institutes of Health (NIH) R01 EY022086, NIH R21 EY029067, and Timothy William Trout Professorship to A.I., and in part by the Core Grant for Vision Research from the NIH to the University of Wisconsin-Madison (P30 EY016665). Support by NIH R01 EY024995 (BRP) and M.D. Matthews Professorship (BRP) is also acknowledged. Support for E.L.M. was partially provided by the NIH predoctoral training program in Genetics (NIH T32 GM007133). The authors thank the University of Wisconsin Translational Research Initiatives in Pathology laboratory (TRIP), supported by the University of Wisconsin Department of Pathology and Laboratory Medicine, UWCCC (P30 CA014520) and the Office of The Director – NIH (S10OD023526) for use of its facilities and services.

Literature Cited

Adachi, M., M. Abe, T. Sasaki, H. Kato, J. Kasahara *et al.*, 2010 Role of inducible or neuronal nitric oxide synthase in neurogenesis of the dentate gyrus in aged mice. Metab. Brain Dis. 25: 419–424. https://doi.org/10.1007/s11011-010-9224-8

Aggarwal, P., T. C. Nag, and S. Wadhwa, 2007 Age-related decrease in rod bipolar cell density of the human retina: an immunohistochemical study. J. Biosci. 32: 293–298. https://doi.org/10.1007/s12038-007-0029-9

Astle, W. J., H. Elding, T. Jiang, D. Allen, D. Ruklisa *et al.*, 2016 The allelic landscape of human blood cell trait variation and links to common complex disease. Cell 167: 1415–1429.e19. https://doi.org/10.1016/j.cell.2016.10.042

Bernal, G. M., J. S. Wahlstrom, C. D. Crawley, K. E. Cahill, P. Pytel *et al.*, 2014 Loss of Nfkb1 leads to early onset aging. Aging (Albany N.Y.) 6: 931–942. https://doi.org/10.18632/aging.100702

Bonneh-Barkay, D., and C. A. Wiley, 2009 Brain extracellular matrix in neurodegeneration. Brain Pathol. 19: 573–585. https://doi.org/10.1111/j.1750-3639.2008.00195.x

Brakebusch, C., C. I. Seidenbecher, F. Asztely, U. Rauch, H. Matthies *et al.*, 2002 Brevican-deficient mice display impaired hippocampal CA1 long-term potentiation but show no obvious deficits in learning and memory. Mol. Cell. Biol. 22: 7417–7427. https://doi.org/10.1128/MCB.22.21.7417-7427.2002

Brown, G. C., and A. Vilalta, 2015 How microglia kill neurons. Brain Res. 1628: 288–297. https://doi.org/10.1016/j.brainres.2015.08.031

Celio, M. R., and I. Blümcke, 1994 Perineuronal nets – a specialized form of extracellular matrix in the adult nervous system. Brain Res. Brain Res. Rev. 19: 128–145. https://doi.org/10.1016/0165-0173(94)90006-X

Chen, M., and H. Xu, 2015 Parainflammation, chronic inflammation, and age-related macular degeneration. J. Leukoc. Biol. 98: 713–725. https://doi.org/10.1189/jlb.3RI0615-239R

Choi, J. H., C. H. Lee, I. K. Hwang, M. H. Won, J. K. Seong *et al.*, 2007 Age-related changes in ionized calcium-binding adapter molecule 1 immunoreactivity and protein level in the gerbil hippocampal CA1 region. J. Vet. Med. Sci. 69: 1131–1136. https://doi.org/10.1292/jvms.69.1131

Collin, E. C., O. Carroll, M. Kilcoyne, M. Peroglio, E. See *et al.*, 2017 Ageing affects chondroitin sulfates and their synthetic enzymes in the intervertebral disc. Signal Transduct. Target. Ther. 2: 17049. https://doi.org/10.1038/sigtrans.2017.49

Colonna, M., and O. Butovsky, 2017 Microglia function in the central nervous system during health and neurodegeneration. Annu. Rev. Immunol. 35: 441–468. https://doi.org/10.1146/annurev-immunol-051116-052358

Danesh, J., P. Whincup, M. Walker, L. Lennon, A. Thomson *et al.*, 2000 Low grade inflammation and coronary heart disease:

prospective study and updated meta-analyses. BMJ 321: 199–204. https://doi.org/10.1136/bmj.321.7255.199

Deepa, S. S., D. Carulli, C. Galtrey, K. Rhodes, J. Fukuda *et al.*, 2006 Composition of perineuronal net extracellular matrix in rat brain: a different disaccharide composition for the net-associated proteoglycans. J. Biol. Chem. 281: 17789–17800. https://doi.org/10.1074/jbc.M600544200

Dityatev, A., G. Brückner, G. Dityateva, J. Grosche, R. Kleene *et al.*, 2007 Activity-dependent formation and functions of chondroitin sulfate-rich extracellular matrix of perineuronal nets. Dev. Neurobiol. 67: 570–588. https://doi.org/10.1002/dneu.20361

Duncan, B. B., M. I. Schmidt, J. S. Pankow, C. M. Ballantyne, D. Couper *et al.*, 2003 Low-grade systemic inflammation and the development of type 2 diabetes: the atherosclerosis risk in communities study. Diabetes 52: 1799–1805. https://doi.org/10.2337/diabetes.52.7.1799

Eliasieh, K., L. C. Liets, and L. M. Chalupa, 2007 Cellular reorganization in the human retina during normal aging. Invest. Ophthalmol. Vis. Sci. 48: 2824–2830. https://doi.org/10.1167/iovs.06-1228

Foscarin, S., R. Raha-Chowdhury, J. W. Fawcett, and J. C. F. Kwok, 2017 Brain ageing changes proteoglycan sulfation, rendering perineuronal nets more inhibitory. Aging (Albany N.Y.). https://doi.org/10.18632/aging.101256

Fougère, B., E. Boulanger, F. Nourhashémi, S. Guyonnet, and M. Cesari, 2016 Chronic inflammation: accelerator of biological aging. J. Gerontol. A Biol. Sci. Med. Sci. 72: 1218–1225. https://doi.org/10.1093/gerona/glw240

Franceschi, C., and J. Campisi, 2014 Chronic inflammation (inflammaging) and its potential contribution to age-associated diseases. J. Gerontol. A Biol. Sci. Med. Sci. 69: S4–S9. https://doi.org/10.1093/gerona/glu057

Fuchs, M., M. Scholz, A. Sendelbeck, J. Atorf, C. Schlegel *et al.*, 2012 Rod photoreceptor ribbon synapses in DBA/2J mice show progressive age-related structural changes. PLoS One 7: e44645. https://doi.org/10.1371/journal.pone.0044645

Galtrey, C. M., and J. W. Fawcett, 2007 The role of chondroitin sulfate proteoglycans in regeneration and plasticity in the central nervous system. Brain Res. Brain Res. Rev. 54: 1–18. https://doi.org/10.1016/j.brainresrev.2006.09.006

Gaudet, A. D., and P. G. Popovich, 2014 Extracellular matrix regulation of inflammation in the healthy and injured spinal cord. Exp. Neurol. 258: 24–34. https://doi.org/10.1016/j.expneurol.2013.11.020

Hageman, G. S., and L. V. Johnson, 1987 Chondroitin 6-sulfate glycosaminoglycan is a major constituent of primate cone photoreceptor matrix sheaths. Curr. Eye Res. 6: 639–646. https://doi.org/10.3109/02713688709025225

Hayashi, N., K. Tatsumi, H. Okuda, M. Yoshikawa, S. Ishizaka *et al.*, 2007 DACS, novel matrix structure composed of chondroitin sulfate proteoglycan in the brain. Biochem. Biophys. Res. Commun. 364: 410–415. https://doi.org/10.1016/j.bbrc.2007.10.040

Higuchi, H., E. L. Macke, W.-H. Lee, S. Miller, J. C. Xu *et al.*, 2014 Genetic basis of age-dependent synaptic abnormalities in the retina. Mamm. Genome 26: 21–32. https://doi.org/10.1007/s00335-014-9546-7

Ishikawa, M., Y. Sawada, and T. Yoshitomi, 2015 Structure and function of the interphotoreceptor matrix surrounding retinal photoreceptor cells. Exp. Eye Res. 133: 3–18. https://doi.org/10.1016/j.exer.2015.02.017

Jäkel, S., and L. Dimou, 2017 Glial cells and their function in the adult brain: a journey through the history of their ablation. Front. Cell. Neurosci. 11: 24. https://doi.org/10.3389/fncel.2017.00024

Jonas, R. A., T.-F. Yuan, Y.-X. Liang, J. B. Jonas, D. K. C. Tay *et al.*, 2012 The spider effect: morphological and orienting classification of microglia in response to stimuli in vivo. PLoS One 7: e30763. https://doi.org/10.1371/journal.pone.0030763

Karlstetter, M., S. Ebert, and T. Langmann, 2010 Microglia in the healthy and degenerating retina: insights from novel mouse models. Immunobiology 215: 685–691. https://doi.org/10.1016/j.imbio.2010.05.010

Kempuraj, D., R. Thangavel, P. A. Natteru, G. P. Selvakumar, D. Saeed *et al.*, 2016 Neuroinflammation induces neurodegeneration. J. Neurol. Neurosurg. Spine 1: 1003.

Kitagawa, H., 2014 Using sugar remodeling to study chondroitin sulfate function. Biol. Pharm. Bull. 37: 1705–1712. https://doi.org/10.1248/bpb.b14-00613

Kitagawa, H., T. Uyama, and K. Sugahara, 2001 Molecular cloning and expression of a human chondroitin synthase. J. Biol. Chem. 276: 38721–38726. https://doi.org/10.1074/jbc.M106871200

Kõks, S., S. Dogan, B. G. Tuna, H. González-Navarro, P. Potter *et al.*, 2016 Mouse models of ageing and their relevance to disease. Mech. Ageing Dev. 160: 41–53. https://doi.org/10.1016/j.mad.2016.10.001

Kurazono, S., M. Okamoto, J. Sakiyama, S. Mori, Y. Nakata *et al.*, 2001 Expression of brain specific chondroitin sulfate proteoglycans, neurocan and phosphacan, in the developing and adult hippocampus of Ihara's epileptic rats. Brain Res. 898: 36–48. https://doi.org/10.1016/S0006-8993(01)02128-X

Lane P., 1988 Subtle gray (sut); small with kinky tail (skt). Mouse News Lett. 165.

Langmann, T., 2007 Microglia activation in retinal degeneration. J. Leukoc. Biol. 81: 1345–1351. https://doi.org/10.1189/jlb.0207114

Lattin, J. E., K. Schroder, A. I. Su, J. R. Walker, J. Zhang *et al.*, 2008 Expression analysis of G Protein-Coupled Receptors in mouse macrophages. Immunome Res. 4: 5. https://doi.org/10.1186/1745-7580-4-5

Lee, C. H., K.-Y. Yoo, J. H. Choi, O. K. Park, I. K. Hwang *et al.*, 2010 Neuronal damage is much delayed and microgliosis is more severe in the aged hippocampus induced by transient cerebral ischemia compared to the adult hippocampus. J. Neurol. Sci. 294: 1–6. https://doi.org/10.1016/j.jns.2010.04.014

Lee, W.-H., H. Higuchi, S. Ikeda, E. L. Macke, T. Takimoto *et al.*, 2016 Mouse *Tmem135* mutation reveals a mechanism involving mitochondrial dynamics that leads to age-dependent retinal pathologies. eLife 5: e19264. https://doi.org/10.7554/eLife.19264

Lewis, G. P., and S. K. Fisher, 2003 Up-regulation of glial fibrillary acidic protein in response to retinal injury: its potential role in glial remodeling and a comparison to vimentin expression. Int. Rev. Cytol. 230: 263–290. https://doi.org/10.1016/S0074-7696(03)30005-1

Li, Y., K. Laue, S. Temtamy, M. Aglan, L. D. Kotan *et al.*, 2010 Temtamy preaxial brachydactyly syndrome is caused by loss-of-function mutations in chondroitin synthase 1, a potential target of BMP signaling. Am. J. Hum. Genet. 87: 757–767. https://doi.org/10.1016/j.ajhg.2010.10.003

Liets, L. C., K. Eliasieh, D. A. van der List, and L. M. Chalupa, 2006 Dendrites of rod bipolar cells sprout in normal aging retina. Proc. Natl. Acad. Sci. USA 103: 12156–12160. https://doi.org/10.1073/pnas.0605211103

Lund, H., M. Pieber, and R. A. Harris, 2017 Lessons learned about neurodegeneration from microglia and monocyte depletion studies. Front. Aging Neurosci. 9: 234. https://doi.org/10.3389/fnagi.2017.00234

Madeira, M. H., R. Boia, P. F. Santos, A. F. Ambrósio, and A. R. Santiago, 2015 Contribution of microglia-mediated neuroinflammation to retinal degenerative diseases. Mediators Inflamm. 2015: 673090. https://doi.org/10.1155/2015/673090

Maroto, M., J. C. Fernández-Morales, J. F. Padín, J. C. González, J. M. Hernández-Guijo *et al.*, 2013 Chondroitin sulfate, a major

component of the perineuronal net, elicits inward currents, cell depolarization, and calcium transients by acting on AMPA and kainate receptors of hippocampal neurons. J. Neurochem. 125: 205–213. https://doi.org/10.1111/jnc.12159

Mikami, T., and H. Kitagawa, 2013 Biosynthesis and function of chondroitin sulfate. Biochim Biophys Acta 1830: 4719–4733. https://doi.org/10.1016/j.bbagen.2013.06.006

Mrdjen, D., A. Pavlovic, F. J. Hartmann, B. Schreiner, S. G. Utz *et al.*, 2018 High-dimensional single-cell mapping of central nervous system immune cells reveals distinct myeloid subsets in health, aging, and disease. Immunity 48: 380–395.e6 (erratum: Immunity 48: 599). https://doi.org/10.1016/j.immuni.2018.01.011

Pattnaik, B. R., P. K. Shahi, M. J. Marino, X. Liu, N. York *et al.*, 2015 A novel *KCNJ13* nonsense mutation and loss of Kir7.1 channel function causes leber congenital amaurosis (LCA16). Hum. Mutat. 36: 720–727. https://doi.org/10.1002/humu.22807

Pereira, S. S., and J. I. Alvarez-Leite, 2014 Low-grade inflammation, obesity, and diabetes. Curr. Obes. Rep. 3: 422–431. https://doi.org/10.1007/s13679-014-0124-9

Perry, V. H., and C. Holmes, 2014 Microglial priming in neurodegenerative disease. Nat. Rev. Neurol. 10: 217–224. https://doi.org/10.1038/nrneurol.2014.38

Porrello, K., and M. M. Lavail, 1986 Immunocytochemical localization of chondroitin sulfates in the interphotoreceptor matrix of the normal and dystrophic rat retina. Curr. Eye Res. 5: 981–993. https://doi.org/10.3109/02713688608995180

Potter, P. K., M. R. Bowl, P. Jeyarajan, L. Wisby, A. Blease *et al.*, 2016 Novel gene function revealed by mouse mutagenesis screens for models of age-related disease. Nat. Commun. 7: 12444. https://doi.org/10.1038/ncomms12444

Rauch U., X.-H. Zhou, and G. Roos, 2005 Extracellular matrix alterations in brains lacking four of its components. Biochem. Biophys. Res. Commun. 328: 608–617. https://doi.org/10.1016/j.bbrc.2005.01.026

Samuel, M. A., Y. Zhang, M. Meister, and J. R. Sanes, 2011 Age-related alterations in neurons of the mouse retina. J. Neurosci. 31: 16033–16044. https://doi.org/10.1523/JNEUROSCI.3580-11.2011

Sher, G., and M. Naeem, 2014 A novel CHSY1 gene mutation underlies Temtamy preaxial brachydactyly syndrome in a Pakistani family. Eur. J. Med. Genet. 57: 21–24. https://doi.org/10.1016/j.ejmg.2013.11.001

Sorokin, L., 2010 The impact of the extracellular matrix on inflammation. Nat. Rev. Immunol. 10: 712–723. https://doi.org/10.1038/nri2852

Stephenson, E. L., M. K. Mishra, D. Moussienko, N. Laflamme, S. Rivest *et al.*, 2018 Chondroitin sulfate proteoglycans as novel drivers of leucocyte infiltration in multiple sclerosis. Brain 141: 1094–1110. https://doi.org/10.1093/brain/awy033

Tang, T., L. Li, J. Tang, Y. Li, W. Y. Lin *et al.*, 2010 A mouse knockout library for secreted and transmembrane proteins. Nat. Biotechnol. 28: 749–755. https://doi.org/10.1038/nbt.1644

Terzibasi, E., M. Calamusa, E. Novelli, L. Domenici, E. Strettoi *et al.*, 2009 Age-dependent remodelling of retinal circuitry. Neurobiol. Aging 30: 819–828. https://doi.org/10.1016/j.neurobiolaging.2007.08.017

Tian, J., L. Ling, M. Shboul, H. Lee, B. O'Connor *et al.*, 2010 Loss of CHSY1, a secreted FRINGE enzyme, causes syndromic brachydactyly in humans via increased NOTCH signaling. Am. J. Hum. Genet. 87: 768–778. https://doi.org/10.1016/j.ajhg.2010.11.005

van Greevenbroek, M. M., C. G. Schalkwijk, and C. D. A. Stehouwer, 2013 Obesity-associated low-grade inflammation in type 2 diabetes mellitus: causes and consequences. Neth. J. Med. 71: 174–187.

von Bernhardi, R., L. Eugenín-von Bernhardi, and J. Eugenín, 2015 Microglial cell dysregulation in brain aging and neurodegeneration. Front. Aging Neurosci. 7: 124. https://doi.org/10.3389/fnagi.2015.00124

Wilson, D. G., K. Phamluong, W. Y. Lin, K. Barck, R. A. D. Carano *et al.*, 2012 Chondroitin sulfate synthase 1 (Chsy1) is required for bone development and digit patterning. Dev. Biol. 363: 413–425. https://doi.org/10.1016/j.ydbio.2012.01.005

Wu, C., X. Jin, G. Tsueng, C. Afrasiabi, and A. I. Su, 2016 BioGPS: building your own mash-up of gene annotations and expression profiles. Nucleic Acids Res. 44: D313–D316. https://doi.org/10.1093/nar/gkv1104

Xu, H., M. Chen, A. Manivannan, N. Lois, and J. V. Forrester, 2008 Age-dependent accumulation of lipofuscin in perivascular and subretinal microglia in experimental mice. Aging Cell 7: 58–68. https://doi.org/10.1111/j.1474-9726.2007.00351.x

Yu, B., J. Chang, Y. Liu, J. Li, K. Kevork *et al.*, 2014 Wnt4 signaling prevents skeletal aging and inflammation by inhibiting nuclear factor-κB. Nat. Med. 20: 1009–1017 [corrigenda: Nat. Med. 21: 1101 (2015)]. https://doi.org/10.1038/nm.3586

Zhang, G., J. Li, S. Purkayastha, Y. Tang, H. Zhang *et al.*, 2013 Hypothalamic programming of systemic ageing involving IKK-β, NF-κB and GnRH. Nature 497: 211–216. https://doi.org/10.1038/nature12143

Zhao, T., J. Gao, J. Van, E. To, A. Wang *et al.*, 2015 Age-related increases in amyloid beta and membrane attack complex: evidence of inflammasome activation in the rodent eye. J. Neuroinflammation 12: 121. https://doi.org/10.1186/s12974-015-0337-1

Zhou, X. H., C. Brakebusch, H. Matthies, T. Oohashi, E. Hirsch *et al.*, 2001 Neurocan is dispensable for brain development. Mol. Cell. Biol. 21: 5970–5978. https://doi.org/10.1128/MCB.21.17.5970-5978.2001

Communicating editor: J. Schimenti